

K-edge XANES of octahedral aluminum compounds: similarities and differences via the analysis of excitonic properties

Newman Amoyaw,^{1,*} Abezu Agegnehu,^{2,*} Francesco Sottile,^{3,4} Matteo Gatti,^{3,4,5} and M. Laura Urquiza^{3,4}

¹*Department of Physics, School of Physical and Mathematical Sciences,*

College of Basic and Applied Sciences, University of Ghana, Legon, Accra, Ghana

²*Applied Physics Department, Adama Science and Technology University, P.O. Box 1888, Adama, Ethiopia*

³*LSI, CNRS, CEA/DRF/IRAMIS, École Polytechnique, Institut Polytechnique de Paris, F-91120 Palaiseau, France*

⁴*European Theoretical Spectroscopy Facility (ETSF)*

⁵*Synchrotron SOLEIL, L'Orme des Merisiers, Saint-Aubin, BP 48, F-91192 Gif-sur-Yvette, France*

This study presents an *ab initio* investigation of the XANES spectra at the aluminum K edge for three compounds: Al_2O_3 , AlF_3 and AlCl_3 , where the Al atoms share the same oxidation state (III) and are coordinated in an octahedral symmetry. The XANES spectra calculated within the independent-particle approximation reveal significant differences, including shifts in the spectrum onset, variations in the spectral shapes, and the presence of a pre-peak in the case of AlCl_3 , all in correspondence with the behavior of the PDOS of the absorbing atom in the different materials. The origin of the features stems from the specific band structure of each compound. When electron-hole interactions are taken into account through the solution of the Bethe-Salpeter equation, a series of dark and bright excitons with large binding energies and Frenkel character is obtained. The strong excitonic effects lead to the suppression of the pre-peak in AlCl_3 and further accentuate the differences among the three Al K-edge spectra.

I. INTRODUCTION

X-ray absorption spectroscopy, particularly x-ray absorption near edge structure (XANES), is a powerful tool for the structural characterization of materials. XANES provides high sensitivity to the local chemical environment of the absorbing atom and to the medium-range structural organization, yielding valuable information on symmetry [1, 2], coordination number [2–4], bond length [5] and bond angle. Therefore, it serves as a distinctive fingerprint to identify and characterize constituent atoms within a material's structure. XANES can be also used to infer changes in the oxidation state of the absorbing atom. An example is the K edge of Mn, where changes in the oxidation state of Mn from II to IV in a series of compounds yield different chemical shifts [6, 7]. Similarly, in a series of vanadium oxides the energy shifts of the absorption edge and the pre-edge have been observed to be linearly dependent on the valence of the absorbing vanadium atom [8].

The fine structures measured with XANES provide information on the local density of the empty electronic states at the site of the absorbing atom, in the presence of the core hole. In particular, K-edge XANES spectra probe predominantly $s \rightarrow p$ dipole transitions, since monopole ($s \rightarrow s$) and quadrupole ($s \rightarrow d$) terms are normally orders of magnitude smaller. However, a pre-edge related to dipole-forbidden transitions is often present at the K edge of low-Z cations in minerals and oxides. These pre-edge features are determined by multiple factors, including coordination number, local distortion, oxidation state, and the nature of ligands around the absorbing

atom. For example, transition metal compounds with tetrahedral geometries usually exhibit stronger pre-peak intensities than those with octahedral geometries [9–11]. The pre-edge features stem from the density of states the bottom of the conduction band, which in these compounds is composed primarily by the transition metal $3d$ empty states. According to group theory, atomic $p-d$ mixing is forbidden under octahedral symmetry but allowed under tetrahedral symmetry. When absorbing atoms have a tetrahedral or distorted octahedral coordination, this results into an enhancement of the pre-peak intensity, where dipole transitions from the core $1s$ state to the $p-d$ hybridized orbitals at the bottom of the conduction band become possible [12]. A similar behavior has been observed in aluminum compounds and minerals [1–4, 13, 14], where tetrahedral symmetry or local distortions in octahedral geometries enable atomic $s-p$ mixing.

Extensive research has been carried out to correlate K-edge spectral features, particularly in the pre-edge region, with the local chemical environment. However, understanding the spectral shapes in detail remains challenging. For instance, in aluminum compounds with octahedral geometries, six-fold coordinated aluminum exhibits a variety of XANES features. The interplay among the various structural parameters (such as the number of Al sites and the distribution of interatomic distances) complicates the quantitative interpretation of XANES spectra [1, 2]. On the other hand, band-structure effects are also expected to strongly influence the absorption features. In addition, the interactions between the core holes and the electrons excited in the conduction states, also known as excitonic effects, can play a crucial role, leading to substantial shifts in the absorption edge and modifications in absorption intensities. In this context, theoretical studies can provide important information for

* These two authors contributed equally.

the interpretation of spectra by allowing the selective activation or deactivation of specific interactions at play in the materials.

For excitations from deep core states, predicting near-edge structures requires appropriate theoretical methods, capable of reproducing spectral features and excitonic effects. In particular, the interaction between the excited electrons and core holes, highly localized and poorly screened, demands a high-level treatment of electron-hole correlation. Common approaches for XANES spectra, in the so-called *core-hole* or *final-state-rule* approximation [15], typically evaluate a one-electron Fermi Golden rule, with a relaxed final state including a partial or a full core hole at a single atomic site within a supercell. Other methods based on multiplet ligand-field theory [16–18] are very efficient, but are not completely parameter free. Alternatively, XANES spectra can be obtained within linear-response theory through the Bethe-Salpeter equation [19, 20] (BSE) using an all-electron approach. Here, core electrons are treated explicitly within a muffin-tin region around the nuclear positions. The BSE is the state-of-the-art method for calculating optical excitations [20] and is also increasingly used for core-level excitation spectra in solids [21–35].

The present work aims to analyze changes in the K-edge XANES spectra of aluminum compounds and relate them to their crystallographic properties and chemical environments. We have carried out independent-particle and state-of-the-art BSE calculations to obtain XANES spectra at the aluminum K edge for Al_2O_3 , AlF_3 , and AlCl_3 , all containing Al atoms with the oxidation state +3 and octahedral coordination. The results show the limits of the atomic perspective. Distorsions from the ideal octahedral structure coupled with strong excitonic effects make the *ab initio* results crucially needed for a quantitative description and analysis of the aluminum compounds.

The manuscript is organized as follows. In Sec. II we describe the theory for the calculation of the XANES spectra through the BSE and independent-particle approximation (IPA), together with the computational details. In Sec. III we present the results for Al_2O_3 , AlF_3 , and AlCl_3 . Finally, in Sec. IV we draw conclusions and perspectives of the present work.

II. METHODS

A. XANES spectrum from the BSE

The XANES spectra are calculated by solving the Bethe-Salpeter equation (BSE), which gives the density-density response function from the solution of a Dyson-like equation for a two-particle correlation function [19]. Applying the GW approximation [36] and using a statically screened Coulomb interaction W , the BSE can be expressed as an effective two-particle Schrödinger equa-

tion [20]:

$$H^{\text{exc}} A_\lambda = E_\lambda A_\lambda, \quad (1)$$

where H^{exc} is the excitonic Hamiltonian and E_λ are the excitation energies. The excitonic Hamiltonian is given by the sum of the three following terms:

$$H^{\text{exc}} = H^{\text{ipa}} + 2H^x - H^c \quad (2)$$

which are matrices in the basis of transitions that, in the Tamm-Dancoff approximation, are between occupied core states and unoccupied Kohn-Sham orbitals $\varphi_{\mu\mathbf{k}} \rightarrow \varphi_{c\mathbf{k}}$. More specifically, those matrix elements are:

$$H_{c\mu\mathbf{k},c'\mu'\mathbf{k}'}^{\text{ipa}} = E_{\mu\mathbf{k}} \delta_{\mu\mu'} \delta_{cc'} \delta_{\mathbf{k}\mathbf{k}'} \quad (3)$$

$$H_{c\mu\mathbf{k},c'\mu'\mathbf{k}'}^x = \int \varphi_{c\mathbf{k}}^*(\mathbf{r}) \varphi_{\mu\mathbf{k}}(\mathbf{r}) \bar{v}_c(\mathbf{r}, \mathbf{r}') \varphi_{c'\mathbf{k}'}(\mathbf{r}') \varphi_{\mu'\mathbf{k}'}^*(\mathbf{r}') d\mathbf{r} d\mathbf{r}' \quad (4)$$

$$H_{c\mu\mathbf{k},c'\mu'\mathbf{k}'}^c = \int \varphi_{c\mathbf{k}}^*(\mathbf{r}) \varphi_{c'\mathbf{k}'}(\mathbf{r}) W(\mathbf{r}, \mathbf{r}') \varphi_{\mu\mathbf{k}}(\mathbf{r}') \varphi_{\mu'\mathbf{k}'}^*(\mathbf{r}') d\mathbf{r} d\mathbf{r}'. \quad (5)$$

Here $E_{\mu\mathbf{k}} = E_{c\mathbf{k}} - E_{\mu\mathbf{k}}$ are the interband transition energies, \bar{v}_c is the bare Coulomb interaction, calculated without its macroscopic component (i.e., the component $\mathbf{G} = 0$ in reciprocal space is set to 0), and the statically screened Coulomb interaction $W = \epsilon^{-1} v_c$ is obtained within the random-phase approximation (RPA) for the inverse dielectric function ϵ^{-1} . The first term in Eq. (2), H^{ipa} , represents the independent-particle transitions. The repulsive term, H^x , is the exchange electron-hole interaction and is responsible for the local-field effects (LFE) [37, 38]. LFE are important in inhomogeneous systems as they reflect the inhomogeneities in the induced microscopic Hartree potential that counteracts the external perturbation. Finally, the attractive term, $-H^c$, describes the electron-hole attraction.

The XANES spectrum can be obtained from the imaginary part of the macroscopic dielectric function $\text{Im}\epsilon_M(\omega)$ in the long-wavelength limit $\mathbf{q} \rightarrow 0$, which can be calculated from of eigenvectors A_λ and eigenvalues E_λ of the BSE Hamiltonian, Eq. (1), as:

$$\text{Im}\epsilon_M(\omega) = \lim_{\mathbf{q} \rightarrow 0} \frac{8\pi^2}{\Omega q^2} \sum_\lambda \left| \sum_{\mu\mathbf{k}} A_\lambda^{\mu\mathbf{k}} \tilde{\rho}_{\mu\mathbf{k}}(\mathbf{q}) \right|^2 \delta(\omega - E_\lambda), \quad (6)$$

where Ω is the crystal volume and $\tilde{\rho}_{\mu\mathbf{k}}$ are the oscillator strengths:

$$\tilde{\rho}_{\mu\mathbf{k}}(\mathbf{q}) = \int \varphi_{\mu\mathbf{k}-\mathbf{q}}^*(\mathbf{r}) e^{-i\mathbf{q}\mathbf{r}} \varphi_{c\mathbf{k}}(\mathbf{r}) d\mathbf{r}. \quad (7)$$

Each excitonic peak in the spectrum, located at energy E_λ , has an intensity given by the absolute square modulus in Eq. (6). If the intensity is negligibly small, the exciton is said to be dark, and bright otherwise.

In the independent-particle approximation, one could rewrite Eq. (6) simply as:

$$\text{Im}\epsilon_M(\omega) = \lim_{\mathbf{q} \rightarrow 0} \frac{8\pi^2}{\Omega q^2} \left| \sum_{\mu\mathbf{c}\mathbf{k}} \tilde{\rho}_{\mu\mathbf{c}\mathbf{k}}(\mathbf{q}) \right|^2 \delta(\omega - E_{v\mathbf{c}\mathbf{k}}), \quad (8)$$

since the excitonic eigenvectors A_λ , which in Eq. (6) mix independent-particle transitions, become $\delta_{\mu\mu'}\delta_{cc'}\delta_{\mathbf{k}\mathbf{k}'}$ (H^{ipa} is a diagonal matrix). If, additionally, the oscillator strengths $\tilde{\rho}_{\mu\mathbf{c}\mathbf{k}}$ are approximately constant for $s \rightarrow p$ transitions (and zero for all other transitions), then the K-edge XANES spectrum becomes proportional to the p component of the projected density of unoccupied states (PDOS) of the absorbing atom.

B. Computational details

The calculations were performed within an all-electron full-potential linearized augmented plane-wave (FP-LAPW) method, as implemented in `Exciting` code [39]. Kohn-Sham density functional theory (KS-DFT) [40] calculations have been done within the local density approximation (LDA) [41] for the exchange correlation functional. We adopted the experimental crystal structure of the three compounds. α - Al_2O_3 has a rhombohedral structure with lattice parameters [42] $a = 5.128 \text{ \AA}$ and $\alpha = 55.287^\circ$. α - AlF_3 , also with rhombohedral unit cell, has parameters [43] $a = 5.0314 \text{ \AA}$ and $\alpha = 58.6772^\circ$. Finally, AlCl_3 has a monoclinic unit cell with parameters [44] $a = 5.914$, $b = 10.234$, $c = 6.148$ and $\alpha = 108.25^\circ$. The convergency of the ground-state density was achieved using a plane-wave cutoff, $R_{MT}|\mathbf{G} + \mathbf{k}|_{max} = 10$ for AlF_3 and $R_{MT}|\mathbf{G} + \mathbf{k}|_{max} = 9$ for Al_2O_3 and AlCl_3 . Here, R_{MT} is the muffin-tin radius of the anion, O (1.45 Bohr), Cl (1.45 Bohr) and F (1.39 Bohr), which is always smaller than $R_{MT} = 2$ Bohr for Al.

The RPA screening was calculated considering 100 conduction bands and a cutoff in the matrix size given by $|\mathbf{G} + \mathbf{q}|_{max} = 4, 7$ and $6 a_0^{-1}$ for Al_2O_3 , AlF_3 and, AlCl_3 , respectively, maintaining the same cutoff for the wavefunctions as for the ground state.

The BSE calculations for the XANES spectra are performed using a shifted \mathbf{k} -point grid (i.e., not containing high-symmetry \mathbf{k} points), which allows for a quicker convergence of the spectra [45]. The adopted \mathbf{k} -point grids are $8 \times 8 \times 8$ for Al_2O_3 , $10 \times 10 \times 10$ for AlF_3 and $6 \times 6 \times 6$ for AlCl_3 with a (0.05, 0.15, 0.25) shift. In all three cases, we observed slow convergence with respect to the number of empty bands. To achieve accurate results, we had to include 60, 50, and 100 empty bands for Al_2O_3 , AlF_3 , and AlCl_3 , respectively. Finally, the XANES spectra have been plotted using a Lorentzian broadening of 0.1 eV.

III. RESULTS AND DISCUSSION

A. 6-fold coordinated aluminum compounds

We have investigated core excitations at the aluminum K edge in three different compounds, α - Al_2O_3 , α - AlF_3 and AlCl_3 , with the aim of relating their distinctive XANES features to variations in the chemical environment, i.e., the crystal structure and the ligand atom. Therefore, we will first discuss their crystallographic properties and their electronic band structures.

Even if all the three materials contain Al in octahedral centers, their crystal structures exhibit strong differences (see Fig. 1). AlF_3 and Al_2O_3 have a rhombohedral cell (R-3c), with alternate layers of Al and F or O atoms in planes perpendicular to the c axis, forming octahedra linked through faces or vertices, respectively. This results in shorter distances between aluminum planes in Al_2O_3 than in AlF_3 , even though the Al-F distances are shorter than the Al-O distances. On the other hand, AlCl_3 crystallizes in an XCl_3 -type layer lattice with a monoclinic (C2/m) symmetry, like CrCl_3 [46]. In this structure, Cl-Al-Cl layers are stacked along the c axis, with octahedra sharing edges along the plane defined by the ab axis, which leads to first neighbor Al atoms sharing a pair of ligands. Finally, it should be noted that while AlF_3 is composed of perfectly symmetric octahedra, in Al_2O_3 and AlCl_3 , the octahedra are slightly distorted.

These strong differences reflect into the band structures, shown in Fig. 2. Our LDA results for α - Al_2O_3 and α - AlF_3 are in very good agreement with previous KS-DFT calculations [47–50]. We are not aware of previous band-structure calculations for AlCl_3 in the literature.

The bottom conduction band of Al_2O_3 and AlF_3 are characterized by a typical parabolic behavior around the Γ point, primarily composed of Al $4s$ states. The top of the valence band has contributions mostly from $2p$ states of O or F. The LDA bandgap in both cases is located at the Γ point, with values of 6.21 eV for Al_2O_3 and 7.76 eV for AlF_3 .

The band structure of AlCl_3 shows more peculiar features, with weakly dispersing top-valence and two split-off bottom-conduction bands, the latter constituted by poorly hybridized Al $4s$ states, mixed with p states from aluminum and chloride atoms. The LDA bandstructure has an indirect bandgap (between Y and Γ) of 4.99 eV and a direct gap, at the Y point, of 5.07 eV.

B. XANES at the Al K edge

The excitations at the Al K edge involve transitions from the $1s$ state to empty states with predominantly p character, localized at the aluminum absorbing atom. Therefore, before addressing the XANES spectra, it is useful to compare first the p component of the projected density of states (PDOS) on Al atoms in the three compounds, as shown in Fig. 3(a). The dispersion of bottom

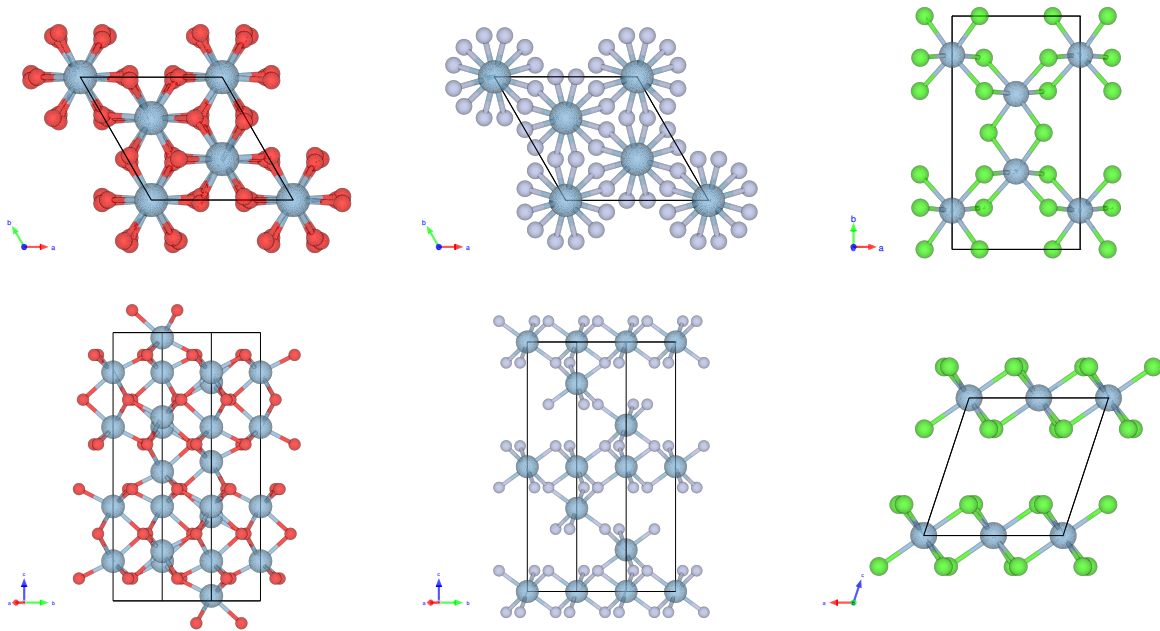


FIG. 1: Top and side views of the crystal structure of α - Al_2O_3 (left) α - AlF_3 (center) and AlCl_3 (right)

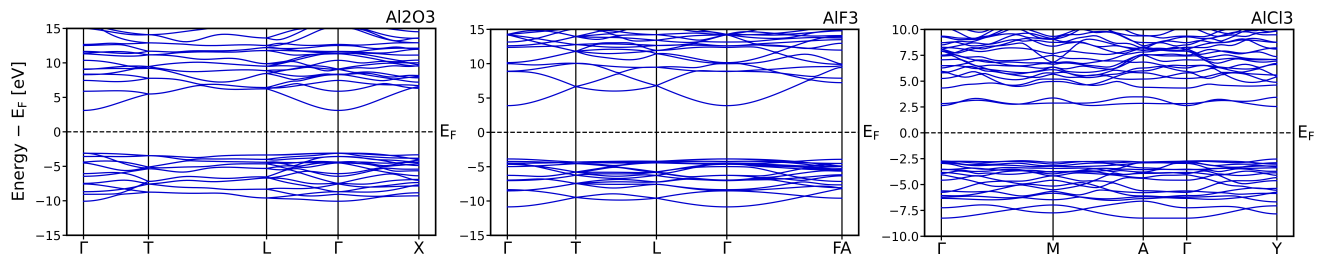


FIG. 2: Band Structure of α - Al_2O_3 (left) α - AlF_3 (center) and AlCl_3 (right), calculated within LDA. The zero of the energy scales has been set at the Fermi energy in the middle of the band gap.

conduction band in Al_2O_3 and AlF_3 , shown in Fig. 2, results in a gradual increase in the p component of the PDOS. In contrast, the low dispersion of the two lowest conduction bands in AlCl_3 is reflected as two sharp peaks in the PDOS. It is interesting to notice that the PDOS shifts towards lower energies, as we go from AlF_3 through Al_2O_3 and AlCl_3 . This trend corresponds to an increasing distortion of the octahedral symmetry around the Al atom, which is known to favor sp hybridization [3], and therefore, the p character in the bottom of the conduction band.

The absorption spectra calculated within the IPA, which, beyond the PDOS, explicitly take into account the oscillator strengths $\tilde{\rho}_{\mu\mathbf{k}}$, are shown Fig. 3(b). In the three cases, the independent-particle spectra follow quite closely the shape of the p empty PDOS of the Al absorbing atom, showing that the oscillator strengths $\tilde{\rho}_{\mu\mathbf{k}}$ are approximately constant. For AlF_3 and Al_2O_3 , the lowest-energy transitions, which are located at the zero of the energy axis of the figure, are dipole forbidden, and

therefore are not visible in any of the three polarization directions. On the contrary, in AlCl_3 there is a pre-peak, which highlights the weak p character of the two non-dispersive bands at the bottom of the conduction band in Fig. 2(c).

The solution of the BSE gives a series of strongly bound dark and bright exciton states with energies below the lowest independent-particle transition energy. The absorption spectra including electron-hole interactions, shown in Fig. 3(c), feature pronounced excitonic peaks, followed by lower-intensity fine structures. These excitons have an atomic nature and a Frenkel character, associated with large binding energies. The comparison between IPA and BSE spectra indicates a dramatic effect of electron-hole interactions, which completely change the spectral shapes, moving their weights to lower energies. At this point, the resemblance with the PDOS is completely lost, showing that an interpretation of XANES spectra based only on a band-structure picture is inadequate.

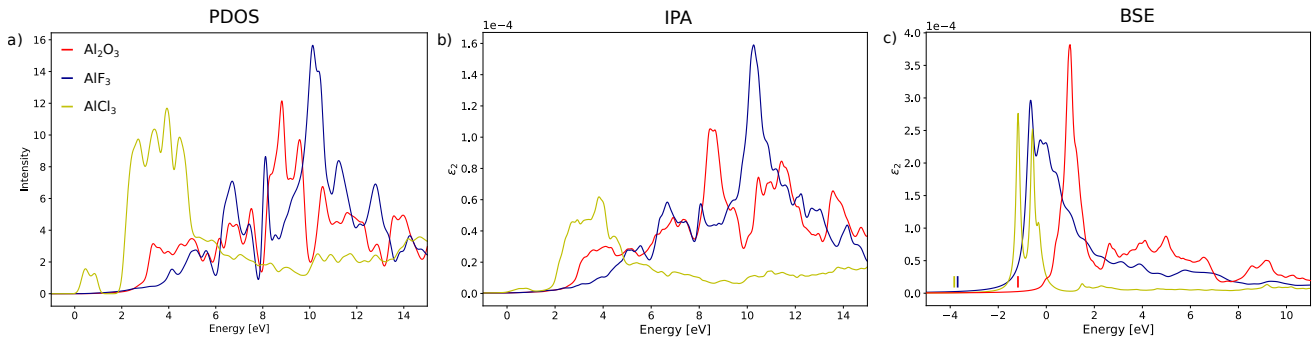


FIG. 3: (a) p component of the PDOS for empty states of aluminum atoms, where the zero of the energy axis has been set to conduction band minimum energy. (b) IPA XANES spectra at the K edge of Al, where the zero has been set at the lowest transition energy of each compound. (c) Bethe-Salpeter XANES spectra at the Al K edge, setting the zero at the lowest IPA transition energy as in (b), in order to highlight the bound character of the exciton states. The IPA and BSE spectra are shown for the in-plane polarization direction, perpendicular to the c axis.

Remarkably, there are no signatures of pre-edge features in any of the three BSE spectra as the lowest-energy excitons are dark even in AlCl₃. Excitonic effects completely suppress the low intensity pre-peak features that are visible in the IPA spectrum in Fig. 3(b). The lowest energy excitons that are dark in all the three compounds are marked with the vertical lines in Fig. 3(c). They have large binding energies: 1.69 eV for Al₂O₃, 4.05 eV for AlF₃, and 4.33 eV for AlCl₃. The calculated BSE absorption spectra of α -Al₂O₃ have been compared in detail with experimental XANES in [51]. To the best of our knowledge, there are no accurate experimental K-edge XANES spectra for the other two compounds. In the following sections, we will focus on AlCl₃, which shows peculiar electronic structure and XANES features.

1. Pre-peak analysis

It is well known that the K-edge XANES spectra of aluminum compounds with tetrahedral coordination have an edge position approximately 2 eV lower than those with octahedral coordination [2, 13]. However, in some cases, a visible pre-edge feature in octahedral aluminum appears at an energy similar to that of the tetrahedral compounds. In particular, in α -Al₂O₃ this pre-peak has been attributed to thermal vibrations that enhance octahedral distortions, allowing further sp hybridization at the bottom of the conduction band [52, 53]. Consequently, calculations including excitonic effects but without coupling to phonons fail to describe this feature, and at best, they only predict a small pre-peak at higher energies, arising from the slight distortions in corundum crystal structure [51]. Non-resonant inelastic x-ray scattering experiments and calculations, which include excitonic effects, capture this pre-peak for high momentum transfer, confirming its non-dipolar nature [51, 54]. The origin of these dark excitations, which in the BSE spectrum result from the mixing of the independent-particle

matrix elements weighted by the excitonic eigenvectors A_λ , are related to two factors: (1) the negligible oscillator strength of the low-energy independent-particle transitions which are dipole forbidden, (2) the cancellation of independent-particle contributions at higher energies when they are summed together [55].

In this work, for AlCl₃ we have found a pre-peak in the IPA spectrum, due solely to electronic contributions, see Fig. 3(b), which is suppressed by electron-hole interactions, as shown by Fig. 3(c). This feature arises from transitions between Al 1s and the bottom of the conduction band with a weak p -character, shown by the PDOS in Fig. 3(a). The origin of the pre-peak is the breaking of the octahedral symmetry around the Al atoms, which allows for sp hybridization. However, when the independent-particle transitions mix together in Eq. (6) to give the BSE spectrum, two prominent peaks and a shoulder emerge at the onset, while suppressing any signature of a pre-peak below them. This raises two important questions: Why is the pre-peak absent in the BSE spectra? What is the nature of the lowest-energy dark and bright excitons?

Fig. 4 illustrates the excitonic weight $|A_\lambda^{\mu\mathbf{k}}|$, projected on the LDA band structure, of each independent particle transition $\mu\mathbf{k} \rightarrow c\mathbf{k}$ contributing to the first dark ($\lambda = 1$) and bright ($\lambda = 5$) excitons. Each independent-particle transition $\mu\mathbf{k} \rightarrow c\mathbf{k}$ is then represented by a circle in the conduction band, with a size proportional to their weight. In both excitons, the most important contributions are given by transitions from core 1s states (out of view in this scale) to the non-dispersive bottom conduction bands. The dark exciton is composed exclusively by these transitions - see top panel - while for the bright exciton transitions from Al 1s to upper conduction bands also sum up - see bottom panel. Moreover, the strong delocalization in reciprocal space of the excitonic weights $|A_\lambda^{\mu\mathbf{k}}|$ suggests a high localization of the exciton in real space, consistent with the typical Frenkel-model picture. From Fig. 3(b), we know that the oscillator strengths,

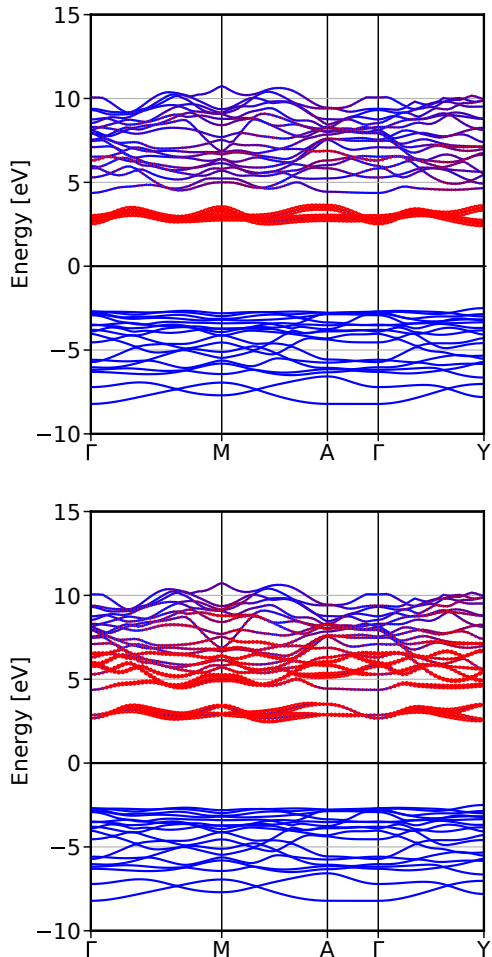


FIG. 4: Contributions of independent transitions to the lowest-energy dark (top) and bright (bottom) excitons.

The size of the circles is proportional to the excitonic coefficients $|A_{\lambda}^{vck}|$.

$\tilde{\rho}_{\mu\mathbf{c}\mathbf{k}}$, for those transitions are dipole allowed. Therefore, each contribution $A_{\lambda}^{\mu\mathbf{c}\mathbf{k}}\tilde{\rho}_{\mu\mathbf{c}\mathbf{k}}$ is separately not zero in Eq. (6). However, the different contributions cancel out when they are summed together and give a dark exciton. This picture contrasts with other materials, including Al_2O_3 , where the strongly bound dark excitons arise instead from zero oscillator strengths $\tilde{\rho}_{\mu\mathbf{c}\mathbf{k}}$.

2. Anisotropy

The anisotropy in the absorption spectra of Al_2O_3 has been extensively studied for core [14, 51, 52] and optical spectra [55, 56], whereas AlF_3 does not exhibit significant directional differences in absorption spectra [49]. Therefore, in the present section we will focus on the more interesting case of AlCl_3 .

AlCl_3 has a strongly anisotropic crystal structure associated to its layered configuration. As a result, the

XANES spectra along the polarization directions xy (perpendicular to the c axis) and z (parallel to the c axis) are quite different, as shown in Fig. 5 for (a) IPA and (b) BSE. In the IPA spectrum, the pre-peak is completely suppressed in the z direction, while at higher energies the spectrum behaves similarly along the two directions. In the BSE spectrum, the two bright excitons in the xy direction, which are split by 0.62 eV and give rise to the two main features, are dark in the z direction. Instead, a single bright exciton is responsible for the main feature in the z polarization, appearing about 0.2 eV higher than the edge in the xy polarization. The origin of this anisotropy is related to the contributions of the first two unoccupied bands to the excitonic peaks. In fact, BSE calculations that explicitly exclude these two empty bands, as shown in Fig. 5(c), yield a series of dark and bright excitons where the anisotropy is strongly reduced, resulting in only a small shift towards lower energies in the z direction.

IV. CONCLUSIONS

In conclusion, we have investigated the XANES spectra of a series of aluminum compounds with octahedral coordination to evaluate the influence of chemical environments on their spectral features. By solving the Bethe-Salpeter equation, to account for excitonic effects in the XANES spectra, we found that the three materials exhibit a strong electron-hole interaction, leading to the formation of localized Frenkel-like excitons with large binding energies. Our analysis reveals that octahedral distortion can be a primary mechanism that allows for sp hybridization, enabling atomic-like dipole transitions $s \rightarrow p$, which are the main contribution to these excitons. Despite this, and in line with other octahedral compounds, the first excitons in all three materials are dark, resulting in the absence of pre-edge features in the calculated XANES spectra. We analyzed in detail the case of AlCl_3 , where two non-dispersive bands at the bottom of the conduction band lead to excitons with noteworthy properties.

Our calculations demonstrate that an atomic perspective alone has strong limitations to analyze the XANES spectra of aluminum in different chemical environments, as the ligand states strongly hybridize with the Al 4s orbitals, significantly influencing the electronic structure. In addition, excitonic effects play a crucial role in determining the edge position and absorption features. As a result, establishing a direct correlation between the differences in the XANES spectra of the three compounds and changes in the chemical environment, through modifications of the ligand atom and variations in the crystal structure, remains challenging.

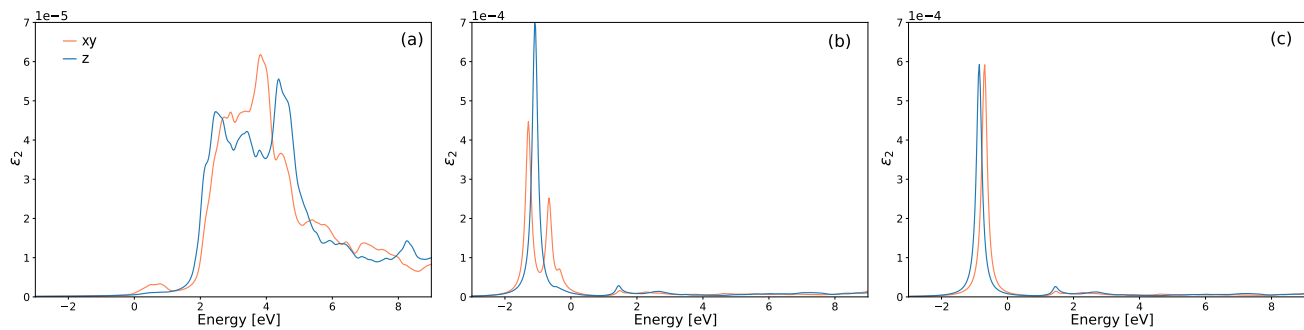


FIG. 5: XANES spectra at the Al K edge in AlCl_3 along two polarization directions xy (perpendicular to the c axis) and z (parallel to the c axes), calculated with (a) the independent particle approximation, (b) the Bethe-Salpeter equation, and (c) with the BSE, but excluding explicitly the two lowest-energy unoccupied bands.

ACKNOWLEDGMENTS

We acknowledge the African School on Electronic Structure: Methods and Applications (ASESMA) where this work was initiated. NA and AA also thank the Palaiseau Theoretical Spectroscopy Group for the kind hospitality through a research stay that was possible

thanks to the “Dispositif de Soutien aux Collaborations avec l’Afrique subsaharienne” of the CNRS, supported also by the Ecole Polytechnique. We acknowledge the French Agence Nationale de la Recherche (ANR) for financial support (Grant Agreements No. ANR-19-CE30-0011). Computational time was granted by GENCI (Project No. 544).

-
- [1] D. Li, G. M. Bancroft, M. E. Fleet, X. H. Feng, and Y. Pan, Al K-edge XANES spectra of aluminosilicate minerals, *American Mineralogist* **80**, 432 (1995), https://pubs.geoscienceworld.org/msa/ammin/article-pdf/80/5-6/432/4222241/am80_432.pdf.
- [2] P. Ildefonse, D. Cabaret, P. Sainctavit, G. Calas, A. M. Flank, and P. Lagarde, Aluminium x-ray absorption near edge structure in model compounds and earth’s surface minerals, *Physics and Chemistry of Minerals* **25**, 112 (1998).
- [3] J. A. van Bokhoven, T. Nabi, H. Sambe, D. E. Ramaker, and D. C. Koningsberger, Interpretation of the al k- and lii/iii-edges of aluminium oxides: differences between tetrahedral and octahedral al explained by different local symmetries, *Journal of Physics: Condensed Matter* **13**, 10247 (2001).
- [4] C. Weigel, G. Calas, L. Cormier, L. Galois, and G. S. Henderson, High-resolution al l2,3-edge x-ray absorption near edge structure spectra of al-containing crystals and glasses: coordination number and bonding information from edge components, *Journal of Physics: Condensed Matter* **20**, 135219 (2008).
- [5] A. Bianconi, E. Fritsch, G. Calas, and J. Petiau, X-ray-absorption near-edge structure of 3d transition elements in tetrahedral coordination: The effect of bond-length variation, *Phys. Rev. B* **32**, 4292 (1985).
- [6] H. Hanson and W. W. Beeman, The mn k absorption edge in manganese metal and manganese compounds, *Phys. Rev.* **76**, 118 (1949).
- [7] M. M. Grush, G. Christou, K. Haemaelaenen, and S. P. Cramer, Site-selective xanes and exafs: A demonstration with manganese mixtures and mixed-valence complexes, *J. Am. Chem. Soc* **117**, 5895 (1995).
- [8] J. Wong, F. W. Lytle, R. P. Messmer, and D. H. Maylotte, k -edge absorption spectra of selected vanadium compounds, *Phys. Rev. B* **30**, 5596 (1984).
- [9] T. Yamamoto, Assignment of pre-edge peaks in k-edge x-ray absorption spectra of 3d transition metal compounds: electric dipole or quadrupole?, *X-Ray Spectrometry* **37**, 572 (2008), <https://analyticalsciencejournals.onlinelibrary.wiley.com/doi/pdf/10.1002/xrs.1000>.
- [10] U. Srivastava and H. Nigam, X-ray absorption edge spectrometry (xaes) as applied to coordination chemistry, *Coordination Chemistry Reviews* **9**, 275 (1973).
- [11] N. Jiang, D. Su, and J. C. H. Spence, Determination of ti coordination from pre-edge peaks in ti k -edge xanes, *Phys. Rev. B* **76**, 214117 (2007).
- [12] T. E. Westre, P. Kennepohl, J. G. DeWitt, B. Hedman, K. O. Hodgson, and E. I. Solomon, A multiplet analysis of fe k -edge $1s \rightarrow 3d$ pre-edge features of iron complexes, *Journal of the American Chemical Society* **119**, 6297 (1997), <https://doi.org/10.1021/ja964352a>.
- [13] D. Cabaret, P. Sainctavit, P. Ildefonse, and A.-M. Flank, Full multiple-scattering calculations on silicates and oxides at the al k edge, *Journal of Physics: Condensed Matter* **8**, 3691 (1996).
- [14] D. Cabaret and C. Brouder, Origin of the pre-edge structure at the al k -edge: The role of atomic vibrations, *Journal of Physics: Conference Series* **190**, 012003 (2009).
- [15] J. J. Rehr, J. A. Soininen, and E. L. Shirley, Final-state rule vs the bethe-salpeter equation for deep-core x-ray absorption spectra, *Physica Scripta* **2005**, 207 (2005).
- [16] F. de Groot, High-resolution x-ray emission and x-ray absorption spectroscopy, *Chemical Reviews* **101**, 1779 (2001).
- [17] F. De Groot and A. Kotani, *Core level spectroscopy of solids* (CRC press, 2008).
- [18] F. M. de Groot, H. Elnaggar, F. Frati, R. pan Wang,

- M. U. Delgado-Jaime, M. van Veenendaal, J. Fernandez-Rodriguez, M. W. Haverkort, R. J. Green, G. van der Laan, Y. Kvashnin, A. Hariki, H. Ikeno, H. Ramanantsoanina, C. Daul, B. Delley, M. Odellius, M. Lundberg, O. Kuhn, S. I. Bokarev, E. Shirley, J. Vinson, K. Gilmore, M. Stener, G. Fronzoni, P. Decleva, P. Kruger, M. Retegan, Y. Joly, C. Vorwerk, C. Draxl, J. Rehr, and A. Tanaka, 2p x-ray absorption spectroscopy of 3d transition metal systems, *Journal of Electron Spectroscopy and Related Phenomena* **249**, 147061 (2021).
- [19] G. Strinati, *Rivista del Nuovo Cimento* **11**, 1 (1988).
- [20] G. Onida, L. Reining, and A. Rubio, Electronic excitations: density-functional versus many-body green's-function approaches, *Rev. Mod. Phys.* **74**, 601 (2002).
- [21] W. Olovsson, I. Tanaka, P. Puschnig, and C. Ambrosch-Draxl, Near-edge structures from first principles all-electron bethe-salpeter equation calculations, *Journal of Physics: Condensed Matter* **21**, 104205 (2009).
- [22] W. Olovsson, I. Tanaka, T. Mizoguchi, P. Puschnig, and C. Ambrosch-Draxl, All-electron bethe-salpeter calculations for shallow-core x-ray absorption near-edge structures, *Phys. Rev. B* **79**, 041102 (2009).
- [23] W. Olovsson, I. Tanaka, T. Mizoguchi, G. Radtke, P. Puschnig, and C. Ambrosch-Draxl, Al $L_{2,3}$ edge x-ray absorption spectra in iii-v semiconductors: Many-body perturbation theory in comparison with experiment, *Phys. Rev. B* **83**, 195206 (2011).
- [24] J. Vinson, J. J. Rehr, J. J. Kas, and E. L. Shirley, Bethe-salpeter equation calculations of core excitation spectra, *Phys. Rev. B* **83**, 115106 (2011).
- [25] J. Vinson and J. J. Rehr, Ab initio bethe-salpeter calculations of the x-ray absorption spectra of transition metals at the l -shell edges, *Phys. Rev. B* **86**, 195135 (2012).
- [26] K. Gilmore, J. Vinson, E. Shirley, D. Prendergast, C. Pemmaraju, J. Kas, F. Vila, and J. Rehr, Efficient implementation of core-excitation bethe-salpeter equation calculations, *Computer Physics Communications* **197**, 109 (2015).
- [27] K. Gilmore, J. Pelliciaro, Y. Huang, J. J. Kas, M. Dantz, V. N. Strocov, S. Kasahara, Y. Matsuda, T. Das, T. Shibauchi, and T. Schmitt, Description of resonant inelastic x-ray scattering in correlated metals, *Phys. Rev. X* **11**, 031013 (2021).
- [28] A. Geondzhian and K. Gilmore, Demonstration of resonant inelastic x-ray scattering as a probe of exciton-phonon coupling, *Phys. Rev. B* **98**, 214305 (2018).
- [29] C. Vorwerk, C. Cocchi, and C. Draxl, Addressing electron-hole correlation in core excitations of solids: An all-electron many-body approach from first principles, *Phys. Rev. B* **95**, 155121 (2017).
- [30] C. Vorwerk, B. Aurich, C. Cocchi, and C. Draxl, Bethe-salpeter equation for absorption and scattering spectroscopy: implementation in the exciting code, *Electronic Structure* **1**, 037001 (2019).
- [31] C. Vorwerk, F. Sottile, and C. Draxl, Excitation pathways in resonant inelastic x-ray scattering of solids, *Phys. Rev. Research* **2**, 042003 (2020).
- [32] C. Vorwerk, F. Sottile, and C. Draxl, All-electron many-body approach to resonant inelastic x-ray scattering, *Phys. Chem. Chem. Phys.* **24**, 17439 (2022).
- [33] J. Vinson, Advances in the ocean-3 spectroscopy package, *Phys. Chem. Chem. Phys.* **24**, 12787 (2022).
- [34] C. D. Dashwood, A. Geondzhian, J. G. Vale, A. C. Pakpour-Tabrizi, C. A. Howard, Q. Faure, L. S. I. Veiga, D. Meyers, S. G. Chiuzbăian, A. Nicolaou, N. Jaouen, R. B. Jackman, A. Nag, M. García-Fernández, K.-J. Zhou, A. C. Walters, K. Gilmore, D. F. McMorrow, and M. P. M. Dean, Probing electron-phonon interactions away from the fermi level with resonant inelastic x-ray scattering, *Phys. Rev. X* **11**, 041052 (2021).
- [35] M. Unzog, A. Tal, and G. Kresse, X-ray absorption using the projector augmented-wave method and the bethe-salpeter equation, *Phys. Rev. B* **106**, 155133 (2022).
- [36] L. Hedin, New Method for Calculating the One-Particle Green's Function with Application to the Electron-Gas Problem, *Phys. Rev.* **139**, A796 (1965).
- [37] N. Wiser, Dielectric constant with local field effects included, *Phys. Rev.* **129**, 62 (1963).
- [38] S. L. Adler, Quantum theory of the dielectric constant in real solids, *Phys. Rev.* **126**, 413 (1962).
- [39] A. Gulans, S. Kontur, C. Meisenbichler, D. Nabok, P. Pavone, S. Rigamonti, S. Sagmeister, U. Werner, and C. Draxl, exciting: a full-potential all-electron package implementing density-functional theory and many-body perturbation theory, *Journal of Physics: Condensed Matter* **26**, 363202 (2014).
- [40] P. Hohenberg and W. Kohn, *Phys. Rev.* **136**, B864 (1964).
- [41] W. Kohn and L. J. Sham, Self-consistent equations including exchange and correlation effects, *Phys. Rev.* **140**, A1133 (1965).
- [42] E. E. Newnham and Y. M. Haan, Refinement of the al_2o_3 , ti_2o_3 , v_2o_3 and cr_2o_3 structures, *Zeitschrift fur Kristallographie - Crystalline Materials* **117**, 235 (1962).
- [43] P. Daniel, A. Bulou, M. Rousseau, J. Nouet, J. L. Fourquet, M. Leblanc, and R. Burriel, A study of the structural phase transitions in alf_3 : X-ray powder diffraction, differential scanning calorimetry (dsc) and raman scattering investigations of the lattice dynamics and phonon spectrum, *Journal of Physics: Condensed Matter* **2**, 5663 (1990).
- [44] S. I. Troyanov, Cheminform abstract: Crystal structure of $ti(alcl_4)_2$ and refinement of the crystal structure of $alcl_3$, *ChemInform* **23** (1992), <https://onlinelibrary.wiley.com/doi/pdf/10.1002/chin.199243008>.
- [45] L. X. Benedict, E. L. Shirley, and R. B. Bohn, Optical absorption of insulators and the electron-hole interaction: An ab initio calculation, *Phys. Rev. Lett.* **80**, 4514 (1998).
- [46] J. A. A. Ketelaar, C. H. MacGillavry, and P. A. Renes, The crystal structure of aluminium chloride, *Recueil des Travaux Chimiques des Pays-Bas* **66**, 501 (1947), <https://onlinelibrary.wiley.com/doi/pdf/10.1002/recl.19470660805>.
- [47] J. Navarro, E. Albanesi, R. Vidal, and J. Ferrón, A study on the structural, electronic and optical properties of the α - alf_3 compound, *Materials Research Bulletin* **83**, 615 (2016).
- [48] H. B. Hamed, A. Qteish, N. Meskini, and M. Alouani, Calculated hybrid and semilocal functionals and gw electronic structure of the metal trifluorides mf_3 ($m = Sc, y, al$), *Phys. Rev. B* **92**, 165202 (2015).
- [49] Y.-R. Chen, V. Perebeinos, and P. B. Allen, Density-functional study of the cubic-to-rhombohedral transition in $\alpha - alf_3$, *Phys. Rev. B* **69**, 054109 (2004).
- [50] A. G. Marinopoulos and M. Grüning, Local-field and excitonic effects in the optical response of α -alumina, *Phys. Rev. B* **83**, 195129 (2011).
- [51] M. L. Urquiza, M. Gatti, and F. Sottile, Connections

- between resonant inelastic x-ray scattering and complementary x-ray spectroscopies: Probing excitons at the $L_{2,3}$ and $L_{1,2}$ edges of α - Al_2O_3 , [Phys. Rev. B **109**, 115157 \(2024\)](#).
- [52] D. Manuel, D. Cabaret, C. Brouder, P. Sainctavit, A. Bordage, and N. Trcera, Experimental evidence of thermal fluctuations on the x-ray absorption near-edge structure at the aluminum k edge, [Phys. Rev. B **85**, 224108 \(2012\)](#).
- [53] J. L. Fulton, N. Govind, T. Huthwelker, E. J. Bylaska, A. Vjunov, S. Pin, and T. D. Smurthwaite, Electronic and chemical state of aluminum from the single- (k) and double-electron excitation ($k\ell$ and $k\ell\ell$) x-ray absorption near-edge spectra of α -alumina, sodium aluminate, aqueous $\text{Al}^{3+} \cdot (\text{H}_2\text{O})_6$, and aqueous $\text{Al}(\text{OH})_4^-$, [The Journal of Physical Chemistry B **119**, 8380 \(2015\)](#).
- [54] S. Delhommaye, G. Radtke, C. Brouder, S. P. Collins, S. Huotari, C. Sahle, M. Lazzeri, L. Paulatto, and D. Cabaret, Assessing temperature effects on multipole contributions and angular dependence in core-level spectroscopies, [Phys. Rev. B **104**, 024302 \(2021\)](#).
- [55] M. L. Urquiza, M. Gatti, and F. Sottile, Pseudopotential bethe-salpeter calculations for shallow-core x-ray absorption near-edge structures: Excitonic effects in α - Al_2O_3 , [Phys. Rev. B **107**, 205148 \(2023\)](#).
- [56] A. G. Marinopoulos and M. Grüning, Local-field and excitonic effects in the optical response of α -alumina, [Phys. Rev. B **83**, 195129 \(2011\)](#).